

Knockout of the Nogo-B Gene Attenuates Tumor Growth and Metastasis in Hepatocellular Carcinoma¹



Bo Zhu*, Shaobo Chen*, Xiaoding Hu*, Xiaofeng Jin*, Yichen Le*, Lihuan Cao*, Zhonghua Yuan[‡], Zhen Lin[¶], Songmin Jiang*, Lichun Sun^{*†,§} and Long Yu*

*State Key Laboratory of Genetic Engineering, Collaborative Innovation Center for Genetics and Development, School of Life Sciences, Fudan University, 2005 Songhu Road, Shanghai 200433, China; [†]Hunan Province Cooperative Innovation Center for Molecular Target New Drug Study, Institute of Pharmacy & Pharmacology, University of South China, Hengyang 421001, China; [‡]Institute of Cardiovascular Disease, Key Laboratory for Arteriosclerosis of Human, University of South China, Hengyang 421001, China; [§]Department of Medicine, School of Medicine, Tulane Health Sciences Center, New Orleans, LA 70112-2699, USA; [¶]Department of pathology, School of Medicine, Tulane Health Sciences Center, New Orleans, LA 70112-2699, USA

Abstract

Human hepatocellular carcinoma (HCC) is a malignant cancer. It is a challenge to develop anti-HCC drugs due to HCC's extreme aggressiveness and with the sensitivity of the liver to show severe adverse effects. More importantly, the precise mechanisms causing HCC pathogenicity are not known. Our previous study disclosed Nogo-B as a reticulon 4 (Rtn4) family member. In the present study, we first identified that Nogo-B played a critical role in HCC progression. We found, *via in vitro* and *in vivo* assays, that Nogo-B was expressed aberrantly in primary HCC tumor tissues and immortal HCC cells but was relatively scarce in the normal liver tissues or cells. Nogo-B knockout, *via* the CRISPR-Cas9 technique, resulted in significant suppression of HCC cell proliferation and tumor growth. Next-generation sequencing analysis showed that Nogo-B knockout have effects on interleukin-6 (IL-6) signaling pathway. Furthermore, we observed that IL-6 induced phosphorylation of STAT3 (pSTAT3) in wild-type HCC cells, but Nogo-B knockout could reduce IL-6-induced increase of pSTAT3, supporting that Nogo-B affects HCC tumor progression possibly *via* regulating the IL-6/STAT3 signaling pathway. In conclusion, Nogo-B is expressed aberrantly in HCCs and plays an oncogenic role. These findings support that Nogo-B may be a novel anti-HCC therapeutic target.

Neoplasia (2017) 19, 583–593

Abbreviations: HCC, hepatocellular carcinoma; IHC, immunohistochemistry; RTN, reticulon; IL-6, interleukin-6; H&E, hematoxylin and eosin; STAT3, signal transducer and activator of transcription factor 3; WT, wild type; FBS, fetal bovine serum; DMEM, Dulbecco's modified Eagle's medium.

Address all correspondence to: Long Yu or Lichun Sun or Songmin Jiang, State Key Laboratory of Genetic Engineering, Collaborative Innovation Center for Genetics and Development, School of Life Sciences, Fudan University, 2005 Songhu Road, Shanghai 200433, China.
E-mail: smjiang@fudan.edu.cn

¹ Financial support: This work was supported by the National Basic Research Program of China (973 Program; 2013CB910504) and the National Key Sci-Tech Special Project of China (2013ZX10002010).

Received 18 December 2016; Revised 10 February 2017; Accepted 15 February 2017

© 2017 The Authors. Published by Elsevier Inc. on behalf of Neoplasia Press, Inc. This is an open access article under the CC BY-NC-ND license (<http://creativecommons.org/licenses/by-nc-nd/4.0/>).
<http://dx.doi.org/10.1016/j.neo.2017.02.007>

Introduction

Liver cancer is the sixth most common cancer and the second leading cause of cancer deaths worldwide, with high incidences in sub-Saharan Africa and Southeast Asia [1–3]. Most (70%–90%) of these liver cancers belong to malignant hepatocellular carcinoma (HCC) [2,3]. Great efforts have been made in the treatment of HCC progression, particularly in HCC recurrence and metastasis after surgery. However, the HCC treatments are limited due to severe toxic sideeffects, with sorafenib being the only FDA-approved anti-HCC drug [4]. The HCC-associated molecular mechanisms scarcely are known. This hinders scientists in their search efforts for new anti-HCC drugs.

There are a variety of genes and their associated signaling pathways that affect HCC progression [4], including the discovery of the involvement of novel genes like nuclear receptor NR4A2 and reticulon 4B (Nogo-B) [5–7]. Previously, we cloned Nogo-B and found that Nogo-B was a reticulon (Rtn) family member [5]. Nogo-B and the Rtn family, including Rtn1, Rtn2, Rtn3 and Rtn4, are evolutionarily conserved and are primarily localized in the endoplasmic reticulum [6,8]. Nogo-B is encoded by gene Rtn4, along with two other isoforms, Nogo-A and Nogo-C. Each isoform displays differences in distribution and function. Nogo-A is expressed highly in the central nervous system and acts as an inhibitor of axonal growth and repair [9,10]. Nogo-C is expressed more in differentiated muscle fibers and brains [11–13]. Nogo-C's functions are not clear, but we found that it was related to HCC growth by acting as a tumor suppressor [14].

Nogo-B is expressed widely in tissues like liver, kidney, and lung [15–17]. Nogo-B plays critical roles in vascular remodeling [18], cell migration and proliferation [19–21], and the epithelial-mesenchymal transition [22]. However, its role in the liver and liver cancers is not fully understood. Growing evidence shows that Nogo-B is strongly related to the liver. In mouse models, Nogo-B was reported to promote liver fibrosis through activation of the transforming growth factor- β signaling pathway [17]. As reported, Nogo-B also increased hepatocyte proliferation induced by hepatocyte growth factor and decreased proliferation suppression induced by transforming growth factor- β 1 [23], with its absence facilitating cell apoptosis in hepatic stellate cells [17,24]. However, there is little known about the role of Nogo-B in HCC progression and metastasis.

Our preliminary data suggested that Nogo-B might play a role in HCC progression. In the present study, we further investigated the expression pattern and the biological functions of Nogo-B in HCC. We found that Nogo-B was overexpressed highly in HCC tissues/cells in comparison with that in normal liver tissues/cells. We further demonstrated that Nogo-B played a critical oncogenic role in growth and metastasis of HCC cells *in vitro* and xenograft tumors model *in vivo*. Furthermore, Nogo-B knockout inhibited HCC cells proliferation, as well as attenuated tumorigenicity and metastasis. These findings suggest that Nogo-B can be considered as a potential therapeutic target for the development of anti-HCC drugs.

Methods

Tumor Specimens

Surgical resection specimens, including primary HCC tumor tissues and the neighboring nontumorous liver tissues, were obtained from HCC patients at the Qidong Liver Cancer Institute (Jiangsu, China) and Zhongshan Hospital (Shanghai, China). All samples were immediately frozen in liquid nitrogen after surgery and later stored at -80°C before further analysis.

Cell Culture and Transfection

Human HCC cell lines (HepG2, Hep3B, SMMC-7721, QGY-7703, MHCC-97H, and HCC-LM3), human glioma cell line U251, and mouse embryonic fibroblast cell line NIH 3T3 were cultured and maintained in Dulbecco's modified Eagle's medium (DMEM) with 10% (v/v) fetal bovine serum (FBS) (Gibco, USA) at 37°C . Cell transfection was performed following the manufacturer's instructions. For Nogo-B knockout, the guide RNA sequence was CACGAACTGGTACTTGAACG, which was designed using the website software from Massachusetts Institute of Technology (USA) (<http://crispr.mit.edu/>). The plasmid pGK1.1 used was obtained from Dr. Zhang's laboratory (Massachusetts Institute of Technology, USA). Western blot assay was applied to select the cells with Nogo-B knockout. DNA sequencing was eventually used for further confirmation. Genomic DNA was extracted. A 699-bp polymerase chain reaction (PCR) amplicon flanking the CRISPR-Cas9-targeted sites (CGTTCAAGTACCAGTTCGTG) was generated using the primers 5'-AGTCCCTGCCCTCCCCTGGGAGGGTGAGTCACG-3' and 5'-GGGAGCTTGAGGGCGAGACTGCGGCAGCAGACAG-3'. The PCR product was purified and ligated into pMD18-T vector (developed by Dr. TaKaRa) following the manufacturer's protocol. The recombinant plasmids were introduced into competent DH5 α cells with ampicillin used for selection. Plasmid DNA was extracted and sequenced across the insert using one of the PCR primers.

Colony Formation Assay and Cell Proliferation Assay

Cells were seeded in six-well plates (1000 cells/well). After incubation for 12 days, the colonies that formed were washed with cold PBS buffer, fixed with 4% paraformaldehyde for 15 minutes, and then stained with 0.2% (w/v) crystal violet for 30 minutes. The colonies were quantified with the Image J software. A cell proliferation assay was performed using Cell Counting Kit-8 according to the manufacturer's protocol (Dojindo Laboratories, Japan). Eight hundred cells per well were grown in 96-well plates and incubated for different times. Cells were treated and stained. Fluorescence was measured at each time point.

Western Blotting

The cell and tissue lysates were subjected to sodium dodecyl sulfate polyacrylamide gel electrophoresis. Proteins were transferred onto nitrocellulose membranes (Millipore, Bedford, MA). These membranes were then blocked in Tris-buffered saline (pH 7.4) containing 5% nonfat milk and 0.1% Tween-20, incubated with primary antibodies for 2 hours at room temperature (RT), washed three times (5 minutes each) in Tris-buffered saline containing 0.1% Tween-20, and followed by incubation with the secondary antibody for 1 hour at RT. The membranes were washed three times (15 minutes each). Immunoreactivity was visualized by enhanced chemiluminescence (GE Healthcare, NJ). The antibodies used include anti-STAT3 (ab68153, Abcam), anti-pSTAT3 (S727) (ab32143, Abcam), anti-Nogo (N-18) (sc-11,027, Santa Cruz), Nogo-A (ab620024, Abcam), and β -actin (cat. # 612656, BD Biosciences).

Quantitative Reverse Transcriptase Polymerase Chain Reaction (qRT-PCR) in Clinical HCC Specimens

Total RNA was extracted from the frozen pulverized tissues using Trizol (Invitrogen), and cDNA synthesis was performed using the Superscript RT kit (TOYOBO, Japan) according to the manufacturer's instructions. qRT-PCR analysis was conducted using the SYBR Green Supermix kit (Toyobo, Osaka, Japan) in combination with

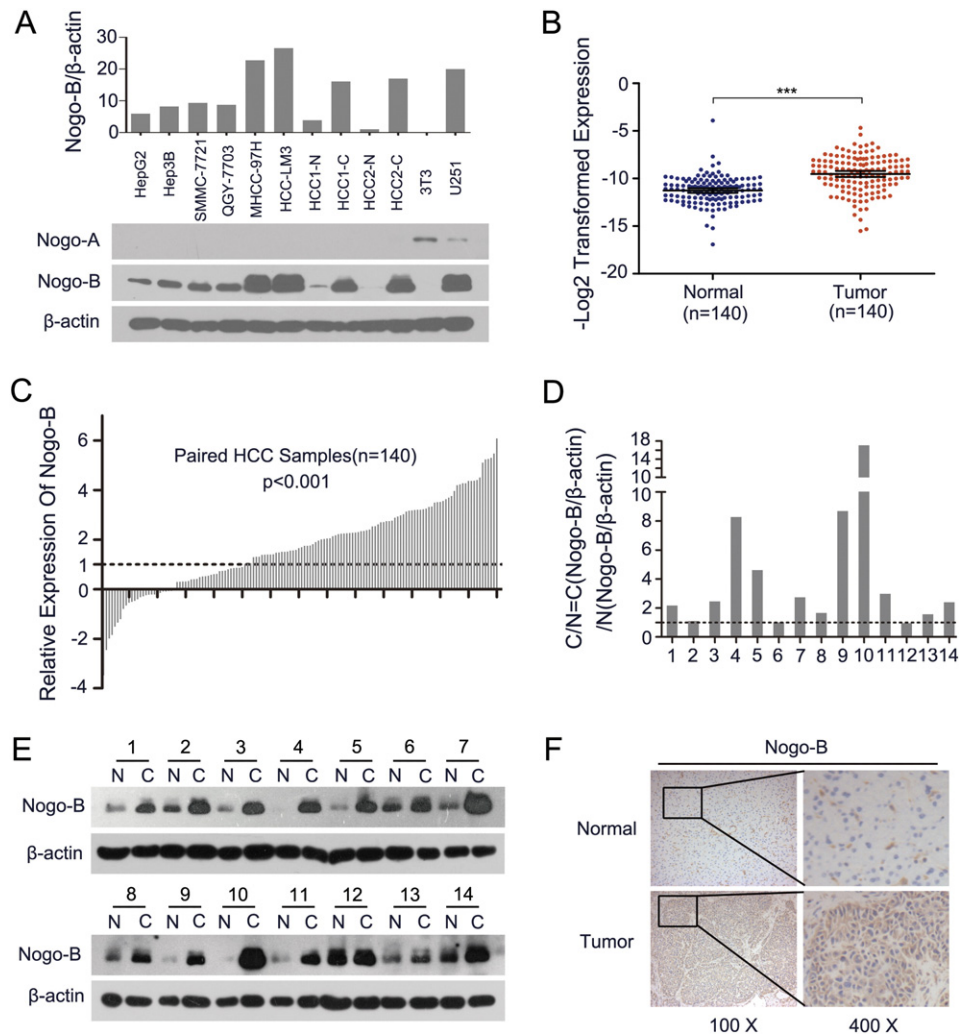


Figure 1. The expression of Nogo-B is upregulated in primary HCC tumor tissues and HCC cell lines. (A) The expressions of Nogo-A and Nogo-B were assayed by Western blotting in HepG2, Hep3B, SMMC-7721, QGY-7703, MHCC-97H, HCC-LM3, HCC1-N, HCC1-C, HCC2-N, HCC2-C, 3T3, and U251 cells plus two representative pairs of HCC and adjacent nontumor liver tissues. Nogo-A was only detected slightly in NIH-3T3 and U251 cells. However, Nogo-B was expressed highly in most HCC cells and HCC tissues, except for NIH-3T3 cells and nontumor liver tissues. (B and C) qRT-PCR analysis shows the mRNA level of Nogo-B in 140 pairs of HCC tumors and the neighboring pathologically nontumor liver tissues (arranged according to relative expression level from low to high), with 64% of HCC tumors showing higher mRNA levels of Nogo-B compared with their nontumor counterparts. Log₂-transformed fold changes of Nogo-B mRNA in HCCs with respect to nontumorous tissues which were normalized to β 2-microglobulin (***) $P < .001$. (D and E) The protein level of Nogo-B was analyzed by Western blot in 14 representative pairs of HCC (HCC tissues and the adjacent nontumor liver tissues). The relative level of Nogo-B protein was quantified using Image J Software. (F) IHC analysis of Nogo-B's expression in HCC tissue and adjacent nontumor liver tissue.

QuantStudio[®] 7 (Life Technologies, USA) according to the manufacturer's instructions. With the paired primers, Nogo-B forward: 5'-GCTCCTCGGGCTCAGTGGTTGTTGAC-3' and reverse: 5'-TGGCCTTCATCTGATTTCTGGATAGC-3', β 2-microglobulin forward: 5'-ATGAGTATGCCTGCCGTGTGAAC-3', and reverse: 5'-TGTGGAGCAACCTGCTCAGATAC-3', A2M forward: 5'-CTATGATTACTACGAGACGGAT-3', and reverse: 5'-CACTTTTCAGCCTTGTGGTC-3', CRP forward: 5'-TCAAAGCCTTCACTGTGTGC-3', and reverse: 5'-AGGTGAGTTGGATCCACAGG-3', VEGF forward: 5'-GGCCTCTGAAACCATGAACT-3', and reverse: 5'-ATGCTGCAGGAAGCTCATCT-3', SOCS3 forward: 5'-CCTGCGCCTCAAGACCTTC-3', and reverse: 5'-GTCAGTGCCTCCAGTAA-3', respectively.

Cell Migration and Invasion Assay

For cell migration assay, cells (2×10^4 cells/well) were seeded into the upper chambers of wells in 24-well plates that had 6.5-mm polycarbonate membranes with an 8- μ m pore size (Corning Inc., NY). For the cell invasion assay, Matrigel matrix in DMEM(1:5) was coated into the upper chambers. The DMEM was removed carefully when the Matrigel matrix was solidified 12 hours later. A total of 2×10^4 cells suspended in serum-free media were seeded into the upper chambers. Medium with 5% FBS was added to the lower chambers as the chemoattractants. Thirty hours later, cells remaining on the upper surfaces of the membranes were removed, with the others that invaded through the membrane filters being fixed with 4% paraformaldehyde for 15 minutes, stained with 0.2% (w/v) crystal violet for 30 minutes, and photographed.

Tumor Xenograft Assay

For tumor growth, wild-type (WT) and Nogo-B knockout (KO) SMMC-7721 cells (2×10^6 cells in 200 μ l PBS) were injected subcutaneously into the right flanks of nude mice 6 weeks old; mice were sacrificed at day 35. Tumors were weighed and the volumes measured. For tumor imaging, QGY-7703 (WT and KO) cells transduced with luciferase viruses were injected subcutaneously into the flanks of nude mice. Tumors were removed once reaching approximately 1.5 cm in diameter and cut into 1- to 2-mm³ pieces, each of which was implanted into the livers of nude mice. Mice were monitored and imaged by Caliper IVIS Lumina II (LB 983 NC100, Berthold Technologies, Germany) on week 1, 3, and 5. The luciferase imaging area was measured by Image J software. Mice were sacrificed at week 8, with tumors, lungs, and livers being removed. Liver intrahepatic metastatic sites and lung metastatic sites were checked and calculated.

Immunofluorescence Staining

Cells were plated previously on chamber slides for 24 hours, then treated with interleukin-6 (IL-6) (R&D systems) for 20 minutes after being starved without serum for 24 hours, and then fixed in 4% paraformaldehyde for 15 minutes at 37°C. Cells were permeabilized with 0.2% Triton X-100 in PBS for 5 minutes and blocked with PBS containing 10% FBS at RT for 1 hour. Cells were incubated with primary antibodies at 4°C overnight and then incubated with secondary antibody and DAPI (Sigma) for 2 hours. Samples were mounted in mounting medium with images taken and analyzed using the Nikon Ni (Nikon, Japan).

Immunohistochemistry (IHC)

For IHC staining, paraffin-embedded tissues were sectioned, mounted on positively charged glass slides (Thermo Scientific, MA), baked, deparaffinized, and rehydrated. Antigen retrieval was completed by heating slides in citrate buffer (10 mmol/L; pH 6.0) for 20 minutes in a pressure cooker. Sections were incubated with primary antibodies overnight at 4°C (Supplementary Figure 1B), washed with PBS, incubated with secondary antibodies (EarthOx, CA) at RT for 30 minutes, and then visualized with an Eclipse Ci-S (Nikon, Japan).

Statistical Analysis

Quantitative data were expressed as mean \pm SE. For comparisons between groups, the two-tailed Student's *t* test was used, with $P < .05$ being statistically significant.

Results

Nogo-B Is Overexpressed in HCCs and Associated with HCC Progression

To investigate the expression profile of Nogo-B, we first investigated the existence of Nogo-A and Nogo-B in eight HCC cell lines and two paired HCC tissues (Figure 1A). We found that Nogo-A was detected only slightly in NIH-3T3 and U251 cells. However, Nogo-B was expressed highly in seven out of eight HCC cell lines and all of the two HCC tissues but was relatively scarce in normal liver tissues. We also examined the expression of Nogo-B at the mRNA level in 140 pairs of HCC tissues by qRT-PCR. We found that Nogo-B was expressed more highly ($P < .001$, Figure 1B) in 113 out of 140 HCC tissues (80.7%, Figure 1C) than in the neighboring nontumorous liver tissues. Furthermore, *via* the clinical-pathological

correlation analysis, we observed that the overexpression of Nogo-B mRNA levels significantly correlated with pathological differentiation ($P = .003$), advanced tumor-lymph node-metastasis stages ($P = .011$), and larger tumor sizes ($P = .034$) (Table 1). We subsequently confirmed the high expression of Nogo-B at the protein level in 14 pairs of tissues (Figure 1, D and E). Western blot analysis showed that Nogo-B protein was expressed aberrantly in 12 out of 14 HCC tissues (85.7%) when compared with nontumorous liver tissues (Figure 1, D and E). These results strongly support that Nogo-B most likely plays a critical role in HCC progression.

Knockout of Nogo-B Suppresses HCC Cells' Proliferation

To investigate the role of Nogo-B in HCCs, we used CRISPR-Cas9 technology to knockout Nogo-B in three HCC cell lines, SMMC-7721 (Figure 2, A, B, and D), QGY-7703 (Figure 2, A, C, and E), and HCC-LM3 (Supplementary Figure 1, D, E, and F), and evaluated the effects of Nogo-B in these cells. The cell colonies with Nogo-B knockout were chosen for further confirmational assays (Supplementary Figure 1, A, B, and C). Cell proliferation assays demonstrated that Nogo-B knockout potently slowed cell proliferation compared with WT cells (Figure 2, D and E). Cell colony assays further identified the similar suppressive effects of Nogo-B knockout. These results implicate the oncogenic role of Nogo-B in HCC tumor progression.

Table 1. The Clinical-Pathological Correlation Analysis of Nogo-B Expression in 140 HCC Tissues

| Characteristic | Nogo-B Expression in HCC | | <i>P</i> Value |
|------------------------------|--------------------------|-------------------|----------------|
| | Low | Moderate and High | |
| Age/year | | | |
| ≥ 50 | 35 | 55 | .292 |
| < 50 | 15 | 35 | |
| Gender | | | |
| Male | 37 | 73 | .325 |
| Female | 13 | 17 | |
| AFP | | | |
| Positive | 27 | 39 | .225 |
| Negative | 23 | 51 | |
| Hepatitis history | | | |
| Positive | 7 | 11 | .763 |
| Negative | 43 | 79 | |
| Tumor size | | | |
| ≥ 5 cm | 19 | 51 | .034 |
| < 5 cm | 31 | 39 | |
| Hepatitis status | | | |
| Positive | 30 | 58 | .602 |
| Negative | 20 | 32 | |
| Pathological differentiation | | | |
| I-II | 43 | 56 | .003 |
| III-IV | 7 | 34 | |
| TNM | | | |
| I-II | 46 | 67 | .011 |
| III-IV | 4 | 23 | |
| Liver cirrhosis | | | |
| Positive | 25 | 53 | .310 |
| Negative | 25 | 37 | |
| Capsular | | | |
| Positive | 40 | 68 | .548 |
| Negative | 10 | 22 | |

Two-tailed Student's *t* test was used. *TNM*, tumor-lymph node-metastasis. Represents *P* values with significant difference.

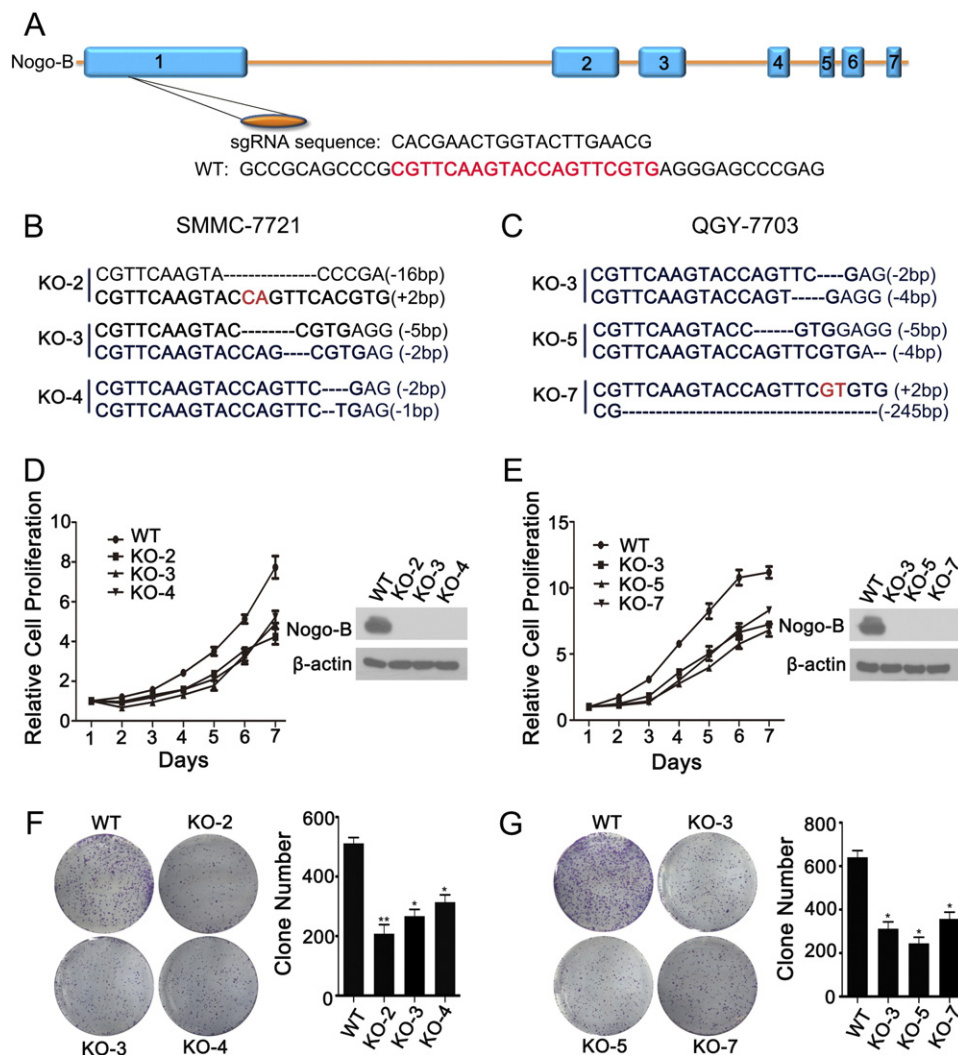


Figure 2. Nogo-B knockout reduces proliferation of HCC cells *in vitro*. (A) The gene structure of Nogo-B in human genome was shown. (B and C) Nogo-B knockout by CRISPR-Cas9 technology in SMMC-7721 and QGY-7703 cells was confirmed by DNA sequencing. (D and E) Nogo-B knockout slows cell proliferation. The suppressive rates in the three Nogo-B-deficient colonies derived from SMMC-7721 cells were 45.15% (KO-2), 36.75% (KO-3), and 32.39% (KO-4) compared with WT cells at day 7. The suppression rates in the three tested colonies from QGY-7703 cells were 35.15% (KO-3), 39.10% (KO-5), and 25.65% (KO-7) at day 7 (F and G) Nogo-B knockout induced significant suppression of colony-forming abilities in either SMMC-7721 or QGY-7703 cells, with the inhibitory rates being 59.28%, 47.81%, and 38.57% in SMMC-7721 KO-2, KO-3, and KO-4 cells and 51.35%, 61.85%, and 44.28% in QGY-7703 KO-3, KO-5, and KO-7 cells. * $P < .05$.

Knockout of Nogo-B Suppresses Tumor Growth

As described above, Nogo-B knockout could suppress HCC cell proliferation *in vitro*. Here, we attempted to determine whether Nogo-B knockout had the same suppressive effects on HCC tumor growth *in vivo*. In HCC SMMC-7721 tumor growth, we found that Nogo-B knockout induced strong tumor suppression (Figure 3A). The tumor volumes at day 35 were 626.98 mm³ in the KO-3 group and 866.02 mm³ in the KO-4 group compared with 2241.01 mm³ in the control group, with the inhibitory rates being 71.02% (KO-3) and 61.36% (KO-4). At day 35, all tumors were removed, photographed (Figure 3B), and weighed (Figure 3C). The average tumor weights in KO-3, KO-4, and control groups were 0.41 g, 0.57 g, and 0.89 g, respectively. Statistical analysis showed significant suppression from the Nogo-B knockout (Figure 3C).

For the effects of Nogo-B on HCC QGY-7703 tumor growth, tumor-imaging assays showed that the average luciferase area at week

1, 3, and 5 was 92.67 mm², 290.53 mm², and 549.99 mm², respectively, in the KO-5 group and 78.43 mm², 420.91 mm², and 961.07 mm², respectively, in the control group (Figure 3, D and E). Statistical analysis showed that the suppressive effects of Nogo-B knockout were significant in week 3 and 5 but not in week 1.

The Effects of Nogo-B on HCC Cell Migration and Invasion

We further did assays to evaluate whether Nogo-B would affect HCC cell migration and invasion in two HCC cells: SMMC-7721 and HCC-LM3. The absence of Nogo-B induced a significant suppression of migration and invasion ability in SMMC-7721 cells, with the inhibitory rates being 52.75% (KO-2), 60.99% (KO-3), and 76.25% (KO-4) in migration and 53.94% (KO-2), 61.60% (KO-3), and 64.98% (KO-4) in invasion (Figure 4, A and C). We also obtained similar suppressive results of Nogo-B knockout in HCC-LM3 cell migration and invasion (Figure 4, B and D).

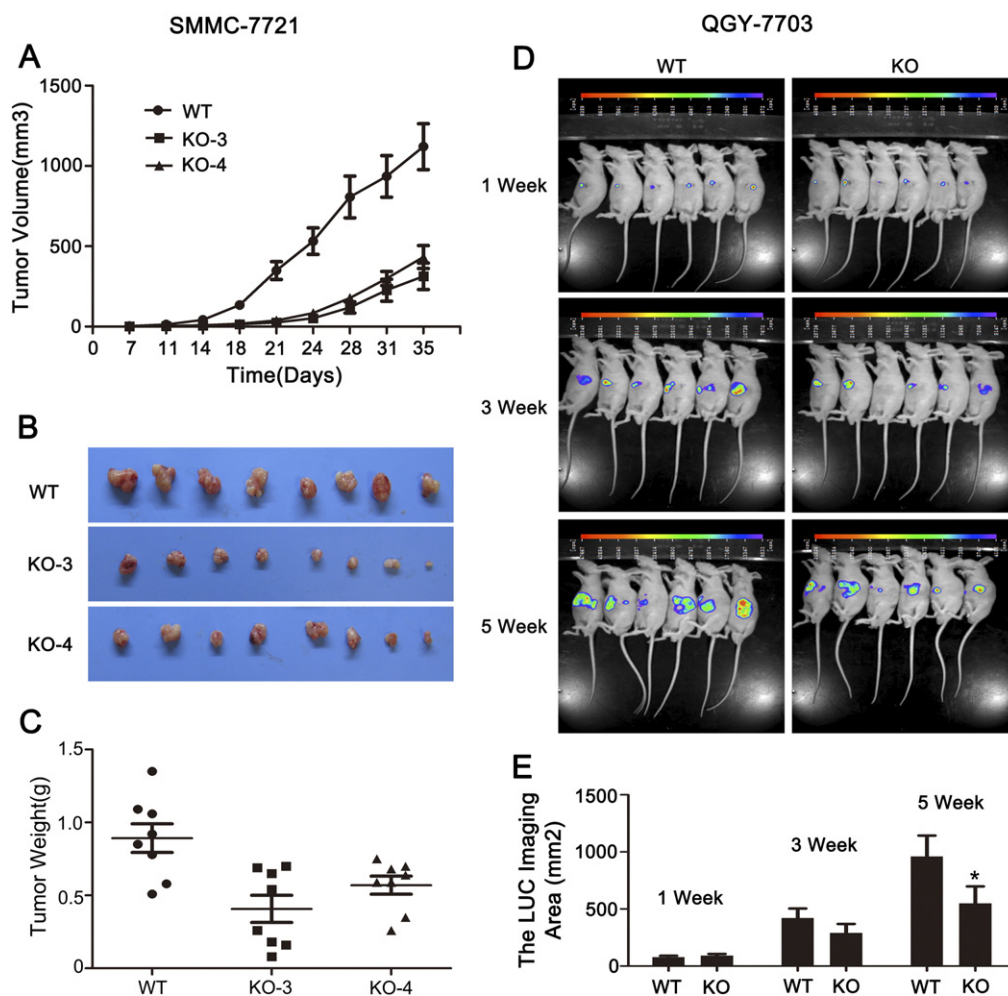


Figure 3. Nogo-B knockout decreases tumorigenicity of HCC cells xenograft model. (A) Tumor volume in the three groups was measured at the indicated days after SMMC-7721 cells (WT, KO-3, and KO-4) injection. (B) The resected tumors from individual nude mice after sacrifice were shown. Eight mice were used in each group. (C) The weight of resected tumors. (D) The growth of orthotopically implanted tumor was monitored using a luminescent imaging technique for 5 weeks. The photograph shows the tumor signal at 1, 3, and 5 weeks after tumor being seeded into the liver. (E) The quantitative data of luciferase imaging area at 1, 3, and 5 weeks after tumor being seeded into the liver. * $P < .05$.

The Effects of Nogo-B on HCC Metastasis In Vivo

To determine the impacts of Nogo-B on HCC metastasis *in vivo*, HCC-LM3 (WT and KO) cells were orthotopically implanted in the livers of nude mice. The metastatic sites in livers and lungs were calculated. The average intrahepatic metastatic sites in livers were 1.2 in the KO group (Nogo-B knockout) and 2.3 in the WT group (Supplementary Figure 2, A and B), with the inhibitory rate being 50.00% (Supplementary Figure 2B). Meanwhile, the average extrahepatic metastatic sites in lungs were 1.3 in the KO group and 2.2 in the WT group (Supplementary Figure 2, D and E), with the inhibitory rate being 38.46% (Supplementary Figure 2E). Hematoxylin and eosin (H&E) staining further showed that Nogo-B knockout resulted in less metastasis in livers (Figure 4E) and lungs in comparison with that of the WT group (Figure 4, E and F; Supplementary Figure 2, C and F). These results suggest the aggressive efficacy of Nogo-B in HCC tumor invasion and metastasis and the potential option for Nogo-B-targeted anti-HCC drug development.

Nogo-B Influences the IL-6/STAT3 Signaling Pathway in HCC Cells

Consequently, we studied the possible Nogo-B-mediated molecular mechanism in HCC cells. We did RNA-seq to analyze the signaling pathways difference among WT cells and KO cells. We found that loss of Nogo-B has effects on IL-6 signaling pathway (Supplementary Figure 3, A, B, and C); an earlier study had reported that Nogo-B promotes hepatocyte proliferation by facilitating the IL-6/STAT3 signaling pathway [23]. We then hypothesized that Nogo-B mediated IL-6 and its downstream signaling networks in HCC cells, possibly with the involvement of STAT3 and its phosphorylation. We then used IL-6 to treat WT SMMC-7721 cells and Nogo-B knockout cells (KO-3 and KO-4). qRT-PCR analysis demonstrated that Nogo-B knockout lead some of the IL6/STAT3 signaling pathway gene A2M, CRP, VEGF, and SOCS3 mRNA level changed in both SMMC-7721 and QGY-7703 cells (Supplementary Figure 3, E and F). Western blot analysis demonstrated that IL-6 induced phosphorylation of STAT3 (pSTAT3) in WT cells, whereas Nogo-B knockout attenuated IL-6-induced phosphorylation in

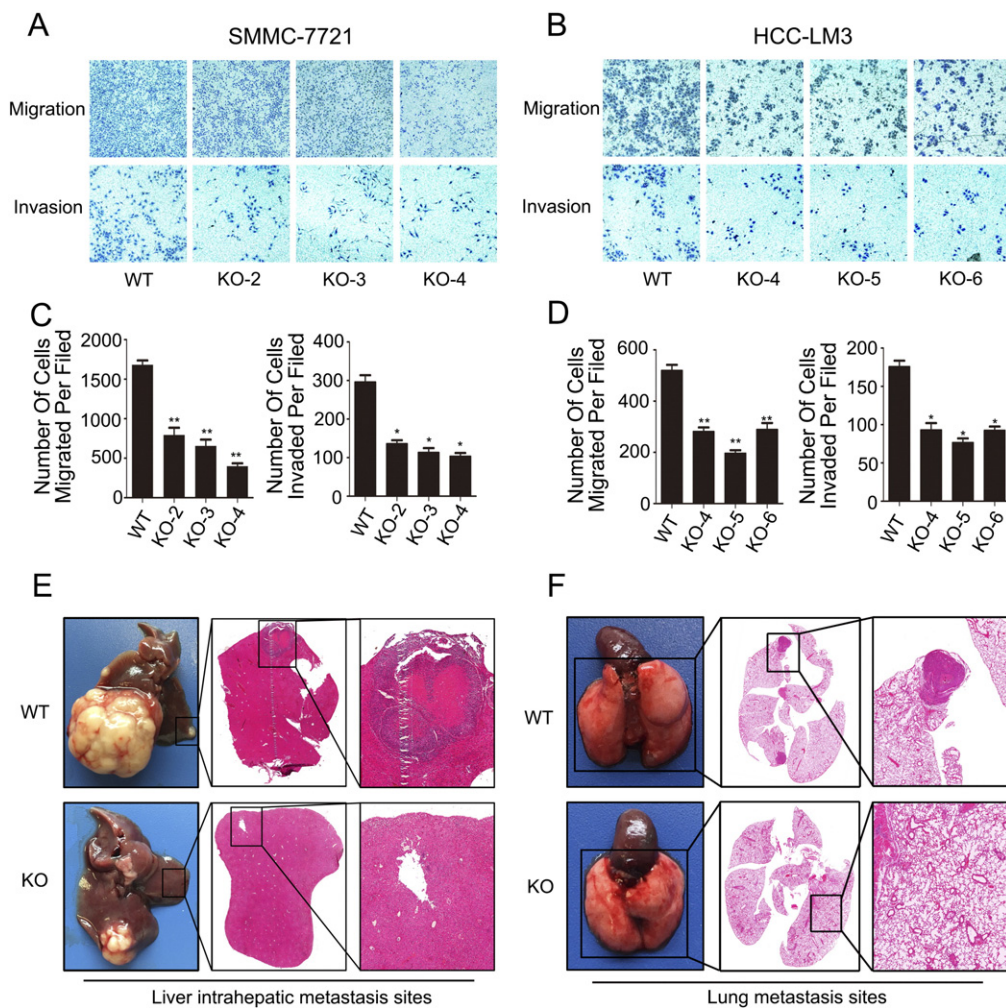


Figure 4. Nogo-B knockout attenuated HCC cells migration and invasion *in vitro* and metastatic ability *in vivo*. (A) Migration and invasion of SMMC-7721 cells (WT, KO-2, KO-3, and KO-4) were determined by Transwell assays. (C) The quantitative data of migration and invasion of SMMC-7721 cells were shown, with the inhibitory rates being 52.75% (KO-2), 60.99% (KO-3), and 76.25% (KO-4) in the migration assay and 53.94% (KO-2), 61.60% (KO-3), and 64.98% (KO-4) in the invasion assay. (B) Migration and invasion abilities of HCC-LM3 cells (WT, KO-4, KO-5, and KO-6) were determined by Transwell assay. (D) The quantitative data of migration and invasion of HCC-LM3 cells, with the inhibitory rates being 45.86% (KO-4), 62.22% (KO-5) and 44.32% (KO-6) in the migration assay and 47.32% (KO-4), 33.27% (KO-5), and 41.39% (KO-6) in the invasion assay. (E) Liver tissues from mouse implanted with HCC-LM3 cells (WT and Nogo-B knockout [KO-5]) by an intrahepatic metastatic assay were stained with H&E. (F) Lung tissues from mouse implanted with HCC-LM3 cells (WT and Nogo-B knockout [KO-5]) by an extrahepatic metastatic assay were stained with H&E. * $P < .05$.

KO-3 and KO-4 cells (Figure 5A). Similar results were observed in WT and KO QGY-7703 cells (KO-5 and KO-7) (Figure 5B). We further examined whether loss of Nogo-B affected nuclear accumulation of IL-6-mediated pSTAT3. We observed that IL-6 induced a high accumulation of pSTAT3 in WT SMMC-7721 cells but not in KO-3 and KO-4 cells (Figure 5C). Similar results were observed in WT and KO QGY-7703 cells (Figure 5D). These findings indicate that loss of Nogo-B impairs IL-6/STAT3 signaling in HCC cells.

Loss of Nogo-B Decreases the Phosphorylation of STAT3 in Primary Liver Tumors

We further investigated whether loss of Nogo-B could result in the decrease of pSTAT3 in liver orthotopic mouse models. SMMC-7721 cells were implanted in mice, and liver tumors were detected. Nogo-B knockout was observed to significantly reduce pSTAT3 and the proliferation marker Ki-67 but not STAT3 (Figure 6A). The inhibitory rates were 31.63% (KO-3) and 29.12% (KO-4) in pSTAT3 and

38.28% (KO-3) and 40.03% (KO-4) in Ki-67 (Figure 6C). We also observed that Nogo-B knockout decreased pSTAT3 and Ki-67 in HCC-LM3 cells but not STAT3 (Figure 6, B and D). The inhibitory rates were 30.12% (KO-5-1) and 28.44% (KO-5-2) in pSTAT3 and 19.38% (KO-5-1) and 20.00% (KO-5-2) in Ki-67 (Figure 6D). These results support that the effects of Nogo-B on HCC tumor progression are possibly by modulating IL-6/STAT3 signaling.

Discussion

It is a tough challenge to develop anti-HCC drugs due to the fact that HCCs are extremely aggressive and livers are unique human organs, easily showing severe adverse effects [4,25–27]. More importantly, the molecular mechanisms are not fully understood in HCCs. Scientists are attempting to determine the precise mechanisms causing HCC pathogenicity and have demonstrated that HCCs are associated strongly with hepatitis and certain other signaling pathways

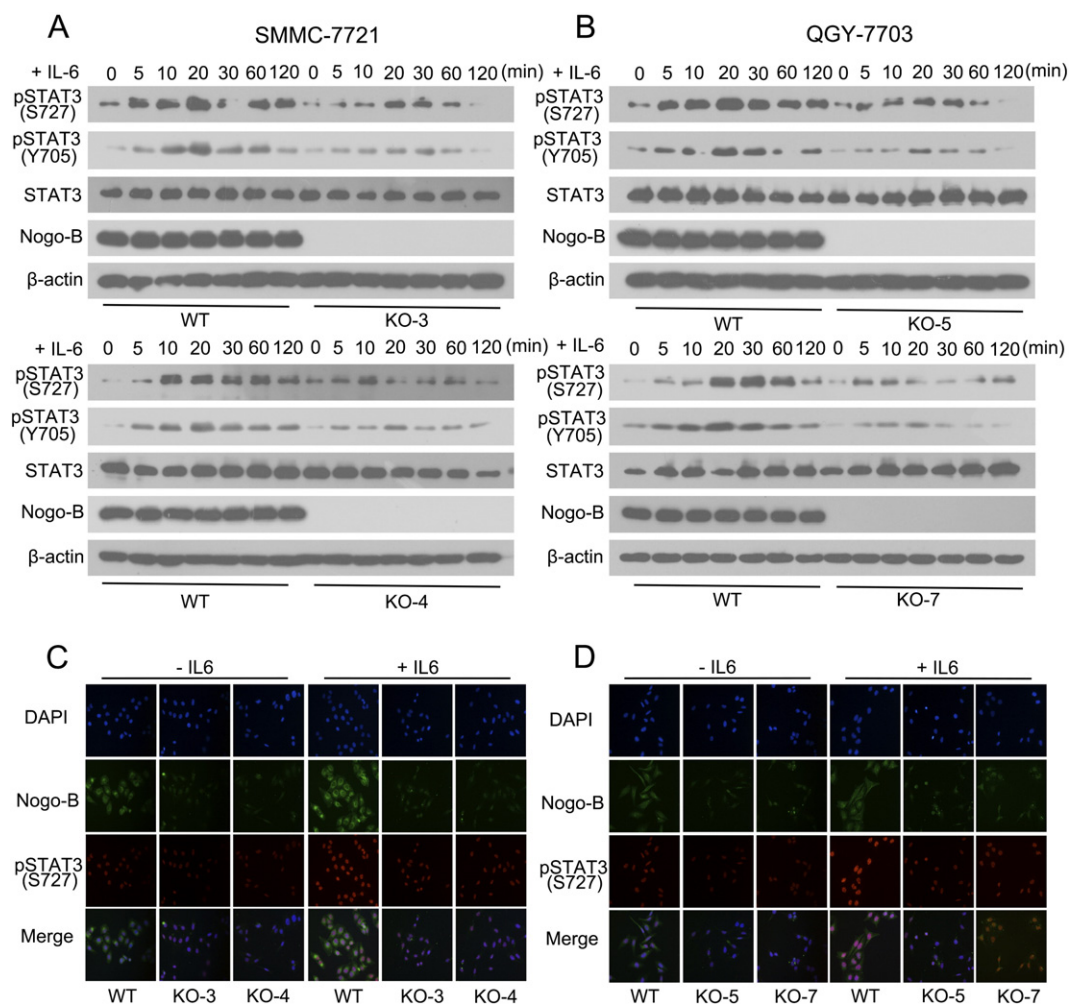


Figure 5. Nogo-B knockout decreases the level of pSTAT3 *in vitro*. (A) SMMC-7721 cells (WT and Nogo-B knockout strains [KO-3 and KO-4]) and (B) QGY-7703 cells (WT and Nogo-B knockout strains [KO-5 and KO-7]) were serum starved for 24 hours and then treated with IL-6 (100 ng/ml) for 0, 5, 10, 20, 30, 60, and 120 minutes. The level of pSTAT3 was measured by Western blot. Nogo-B knockout attenuated the level of pSTAT3. (C) SMMC-7721 cells (WT, KO-3, and KO-4) and (D) QGY-7703 cells (WT, KO-5, and KO-7) were treated with IL-6 (100 ng/ml) for 20 minutes after serum starvation for 24 hours. The accumulation of nuclear pSTAT3 was then determined by immunofluorescence. Nogo-B knockout affected the pSTAT3 accumulation in the nucleus.

such as Wnt signaling and Notch signaling [4,25–28]. Certain genes mutate more frequently in HCCs than in other cancers. Conversely, some others mutate less in HCCs [4,28]. These new discoveries greatly help us to search and develop more effective and specific anti-HCC drugs.

We previously demonstrated that certain genes, like Notch1, Nogo-C, and NR4A2, were involved in HCC progression. We found that Notch1 and NR4A2 are expressed highly in many cancers and potentially act as oncogenic markers [4,29,30] with their interactions in cervical cancers [30] and HCCs (unpublished data). We also identified that Nogo-C acted as a tumor suppressor in HCCs [14]. Conversely, we presently disclosed that Nogo-B might be an oncogene in HCCs, with Nogo-A being undetectable in most HCC cases. These findings provide novel directions for study of the precise molecular mechanism of the Nogo gene family and new strategies to develop potential Nogo-associated anti-HCC drugs.

Nogo-B was discovered in our previous study [5]. Nogo-B exists widely in various tissues [6,11,31]. Nogo-B has demonstrated its biological functions in cell migration [18,32], cell adhesion [18,22,33], vascular remodeling [18], and tissue repair [21].

Nogo-B is also reportedly related to hepatocyte proliferation, liver regeneration, and fibrosis [17,23,24]. However, there is no study to connect Nogo-B with HCCs. To understand the functional role of Nogo-B in HCCs, we first investigated and proved that there is aberrant expression of Nogo-B in primary HCC tissues and immortal HCC cell lines but not in normal liver tissues and cells. Also, Nogo-A is not in normal or pathological tissues/cells, predicting that Nogo-B plays a unique role in HCCs.

Given that Nogo-B aberrantly enhances liver cell proliferation and migration [18,22,32], we hypothesized that Nogo-B might act as an oncogene to enhance HCC development. Our loss-of-function assays showed that loss of Nogo-B reduced HCC cell proliferation and migration and decreased tumor growth and metastasis. On the other hand, the gain-of-function assays showed that overexpression of Nogo-B enhanced cell proliferation and migration (unpublished data). These findings support that Nogo-B plays an oncogenic role in HCCs. To further understand the possibility of Nogo-B-mediated signaling networks, we did RNA-seq assays and found that loss of Nogo-B had effects on IL-6 signaling pathway (Supplementary Figure 3). Nogo-B was reported to promote hepatocyte proliferation by

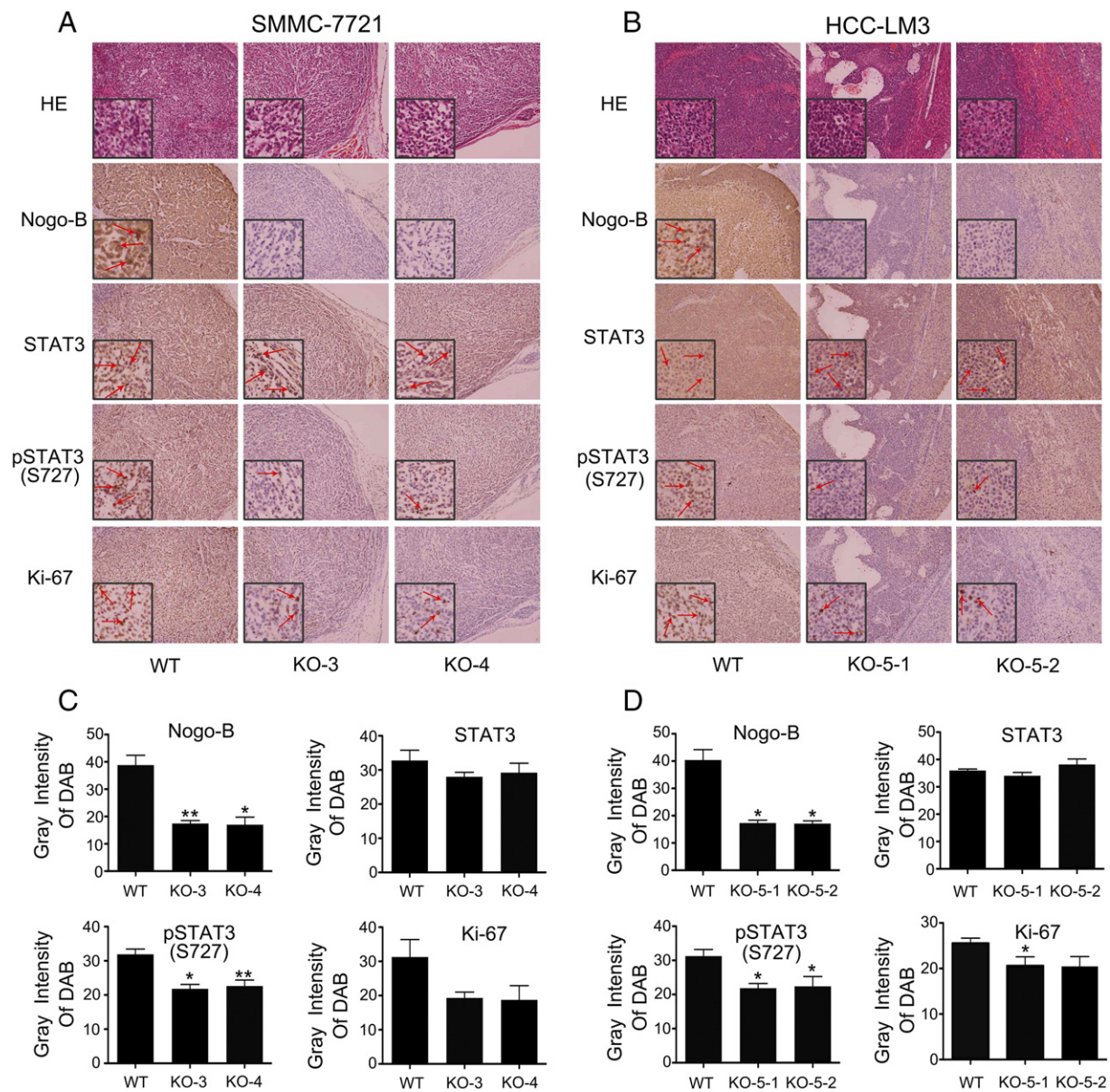


Figure 6. Nogo-B Knockout decreases the pSTAT3 level *in vivo*. (A-B) IHC analysis of proteins as indicated in tumors derived from (A) SMMC-7721 cells (WT, KO-3, and KO-4) and (B) HCC-LM3 cells (WT and KO-5). Loss of Nogo-B attenuated the level of pSTAT3 and Ki-67 in the KO groups compared with the WT group. (C-D) The gray intensities of immunosignals of Nogo-B, STAT3, pSTAT3 (S727), and Ki67 in tumor tissues derived from (C) SMMC-7721 cells (WT, KO-3, and KO-4) and (D) HCC-LM3 cells (WT and KO-5) were semiquantified by image analysis. * $P < .05$, ** $P < .01$.

facilitating the IL-6/STAT3 signaling pathway [23]. Recent study disclosed that IL-6 related to tumor growth and invasion in many types of human cancer [34–39], and IL-6 plays roles during the HCC that represents an inflammation-linked cancer [40,41], abnormal IL-6/STAT3 signaling in cancer cells has emerged as a major mechanism for cancer initiation and development [42–44], STAT3 is constitutively active in most cancer cells [45,46]. Activation of STAT3 is related to cell proliferation and metastasis [47–49]. STAT3 has been found to be constitutively activated by IL-6 in many types of human malignancies [34,45]. IL-6, through p-STAT3 rather than p-STAT1 signal pathway, affects hepatic function and tumor progression, and determines HCC patient survival [50]. These imply that the correlation of Nogo-B and IL-6/STAT3 may play an important role in HCCs [51–53]. Thus, we further focused on the study of Nogo-B signaling and IL-6/STAT3

signaling in HCCs. Our serial assays demonstrated that the new Nogo-B/IL-6/STAT3 signaling pathways indeed participated in HCC development.

We observed that Nogo-B knockout reduced IL-6-induced phosphorylation of STAT3 (pSTAT3) and the nuclear accumulation of pSTAT3 in HCC cells. Nogo-B contains a conserved reticulon homology domain, a 66-aa loop domain termed Nogo-66 in the reticulon homology domain, which can interact with glycosylphosphatidylinositol-linked cell-surface Nogo-66 receptors [54]. Nogo-66 induced astroglial differentiation of NPCs and activated phosphorylation of STAT3 at both Ser727 and Tyr705 and the phosphorylation of mTOR [55]. Nogo-66 influences embryonic stem cell self-renewal and differentiation *via* Stat3 signaling pathway [56]. Nogo-P4, an active segment of Nogo-66, is able to stimulate the

phosphorylation of STAT3 and induce the expression of inducible nitric oxide synthase and cyclooxygenase-2 and the release of proinflammatory cytokines [57,58]. The Nogo-induced activation of NgR on microglia promotes the expression of proinflammatory cytokines and inhibits cell adhesion and migration behaviors [59]. Therefore, we hypothesized that nogo-66/NgR regulated the IL-6/STAT3 signaling pathway. We selected a unique pSTAT3 antibody with its phosphorylation at Ser727 and Tyr705 to analyze the effects of Nogo-B on the phosphorylation of STAT3. The results demonstrated that Nogo-66 might participate in Nogo-B-mediated IL-6/STAT3 signaling via regulating the phosphorylation of STAT3. We will next focus on studies to determine the roles of Nogo-66 in Nogo-B/IL-6/STAT3 signaling networks and the applications for developing new Nogo-B-targeted anti-HCC drugs.

In conclusion, it has been demonstrated that Nogo-B is uniquely overexpressed in HCCs and plays an oncogenic role in HCC progression. Loss of Nogo-B extremely suppressed HCC cell and tumor growth, with gain of Nogo-B inducing HCC cell growth. These findings support that Nogo-B may be a new anti-HCC therapeutic target.

Supplementary data to this article can be found online at <http://dx.doi.org/10.1016/j.neo.2017.02.007>.

Authors' Contributions

Conception and design: B. Z., L. Y., L. C. S.; performed the experiments: B. Z.; analysis and interpretation of data: B. Z., L. Y., L. C. S.; contributed reagents/materials: S. B. C, X. D. H., X. F. J., Y. C. L., S. M. J., Z. L.; wrote the paper: B. Z., S. M. J., L. Y., L. C. S. All authors have read and approved the final manuscript.

Conflict of Interest [5]

The authors declare that they have no competing interests.

Acknowledgements

We thank Dr. Jun Chen (Liver Cancer Institute of Zhongshan Hospital of Fudan University) for his expertise on animal study.

References

- [1] Torre LA, Bray F, Siegel RL, Ferlay J, Lortet-Tieulent J, and Jemal A (2015). Global cancer statistic, 2012. *CA Cancer J Clin* **65**, 87–108.
- [2] Howlader N, Noone A, Krapcho M, Garshell J, Miller D, Altekruse S, Kosary C, Yu M, Ruhl J, and Tatalovich Z (2014). SEER Cancer Statistics Review; 2014 1975–2011.
- [3] McGlynn KA and London WT (2012). International liver cancer incidence trends—letter. *Cancer Epidemiol Biomarkers Prev* **21**, 384–385.
- [4] Sun L, Sun G, Yu Y, and Coy DH (2015). Is notch signaling a specific target in hepatocellular carcinoma? *Anticancer Agents Med Chem* **15**.
- [5] Yang J, Yu L, Bi AD, and Zhao SY (2000). Assignment of the human reticulon 4 gene (RTN4) to chromosome 2p14→2p13 by radiation hybrid mapping. *Cytogenet Cell Genet* **88**, 101–102.
- [6] Oertle T and Schwab ME (2003). Nogo and its paRTNers. *Trends Cell Biol* **13**, 187–194.
- [7] Wang Z (2003). Structure and function of Nurr1 identifies a class of ligand-independent nuclear receptors. *Nature* **423**, 555–560.
- [8] Grandpré T, Nakamura F, Vartanian T, and Strittmatter SM (2000). Identification of the Nogo inhibitor of axon regeneration as a reticulon protein. *Nature* **403**, 439–444.
- [9] Prinjha R, Moore SE, Vinson M, Blake S, Morrow R, Christie G, Michalovich D, Simmons DL, and Walsh FS (2000). Neurobiology: Inhibitor of neurite outgrowth in humans. *Nature* **403**, 383–384.
- [10] Chen MS, Huber AB, Me VDH, Frank M, Schnell L, Spillmann AA, Christ F, and Schwab ME (2000). Nogo-A is a myelin-associated neurite outgrowth inhibitor and an antigen for monoclonal antibody IN-1. *Nature* **403**, 434–439.

- [11] Teng FYH and Tang BL (2008). Cell autonomous function of nogo and reticulons: The emerging story at the endoplasmic reticulum. *J Cell Physiol* **216**, 303–308.
- [12] Josephson A, Widenfalk J, Widmer HW, Olson L, and Spenger C (2001). Nogo mRNA expression in adult and fetal human and rat nervous tissue and in weight drop injury. *Exp Neurol* **169**, 319–328.
- [13] Anding BI, Long YU, Yang J, Zhang M, Zhou Y, and Zhao S (2000). Cloning and expression analysis of human reticulon 4c cDNA. *Chin Sci Bull* **45**, 1862–1869.
- [14] Liu X, Cui SJ, Zhu SJ, Geng DC, and Yu L (2014). Nogo-C contributes to HCC tumorigenesis via suppressing cell growth and its interactome analysis with comparative proteomics research International. *J Clin Exp Pathol* **7**, 2044–2055.
- [15] Marin EP, Moeckel G, Al-Lamki R, Bradley J, Yan Q, Wang T, Wright PL, Yu J, and Sessa WC (2010). Identification and regulation of reticulon 4B (Nogo-B) in renal tubular epithelial cells. *Am J Pathol* **177**, 2765–2773.
- [16] Wright PL, Yu J, Di YP, Homer RJ, Chupp G, Elias JA, Cohn L, and Sessa WC (2010). Epithelial reticulon 4B (Nogo-B) is an endogenous regulator of Th2-driven lung inflammation. *J Exp Med* **207**, 2595–2607.
- [17] Zhang D, Utsumi T, Huang HC, Gao L, Sangwung P, Chung C, Shibao K, Okamoto K, Yamaguchi K, and Groszmann RJ (2011). Reticulon 4B (Nogo-B) is a novel regulator of hepatic fibrosis †. *Hepatology* **53**, 1306–1315.
- [18] Acevedo L, Yu J, Erdjument-bromage H, Miao RQ, Kim JE, Fulton D, Tempst P, Strittmatter SM, and Sessa WC (2004). A new role for Nogo as a regulator of vascular remodeling. *Nat Med* **10**, 382–388.
- [19] Yang YS and Strittmatter SM (2007). The reticulons: a family of proteins with diverse functions. *Genome Biol* **8**, 1–10.
- [20] Paszkowiak JJ, Maloney SP, Kudo FA, Muto A, Teso D, Rutland RC, Westvik TS, Pimiento JM, Tellides G, Sessa WC, and Dardik A (2007). Evidence supporting changes in Nogo-B levels as a marker of neointimal expansion but not adaptive arterial remodeling. *Vascul Pharmacol* **46**, 293–301.
- [21] Yu J, Fernández-Hernando C, Suarez Y, Schleicher M, Hao Z, Wright PL, Dileonzo A, Kyriakides TR, Sessa WC, and Ignarro LJ (2009). Reticulon 4B (Nogo-B) is necessary for macrophage infiltration and tissue repair. *Proc Natl Acad Sci* **106**, 17511–17516.
- [22] Xiao W, Zhou S, Xu H, Li H, He G, Liu Y, and Qi Y (2013). Nogo-B promotes the epithelial-mesenchymal transition in HeLa cervical cancer cells via Fibulin-5. *Oncol Rep* **29**, 109–116 [108].
- [23] Gao L, Teruo U, Keitaro T, Bo L, Zhang D, Scott SE, and Yasuko I (2013). Reticulon 4B (Nogo-B) facilitates hepatocyte proliferation and liver regeneration in mice. *Hepatology* **57**, 1992–2003.
- [24] Tashiro K, Satoh A, Utsumi T, Chung C, and Iwakiri Y (2013). Absence of Nogo-B (Reticulon 4B) facilitates hepatic stellate cell apoptosis and diminishes hepatic fibrosis in mice. *Am J Pathol* **182**, 786–795.
- [25] Hanahan D and Weinberg R (2011). Hallmarks of cancer: the next generation. *Cell* **144**, 646–674.
- [26] El-Serag HB and Rudolph KL (2007). Hepatocellular carcinoma: epidemiology and molecular carcinogenesis. *Gastroenterology* **132**, 2557–2576.
- [27] Thompson EW and Price JT (2005). Mechanisms of tumour invasion and metastasis: emerging targets for therapy. *Expert Opin Ther Targets* **6**, 217–233.
- [28] Sun G, Mackey LV, Coy DH, Yu CY, and Sun L (2014). The histone deacetylase inhibitor vaproic acid induces cell growth arrest in hepatocellular carcinoma cells via suppressing notch signaling. *J Cancer* **6**, 996–1004.
- [29] Sun L and Coy DH (2014). Somatostatin and its analogs. *Curr Drug Targets* , 16.
- [30] Sun L, Liu M, Sun GC, Yang X, Qian Q, Feng S, Mackey LV, and Coy DH (2016). Notch signaling activation in cervical cancer cells induces cell growth arrest with the involvement of the nuclear receptor NR4A2. *J Cancer* **7**, 1388–1395.
- [31] Voeltz GK, Prinz WA, Shibata Y, Rist JM, and Rapoport TA (2006). A class of membrane proteins shaping the tubular endoplasmic reticulum. *Cell* **124**, 573–586.
- [32] Xu W, Hong W, Yan S, Ning Y, Cai Z, and Qiang L (2011). Nogo-B regulates migration and contraction of airway smooth muscle cells by decreasing ARPC 2/3 and increasing MYL-9 expression. *Respir Res* **12**, 1–9.
- [33] Zhou S, Xiao W, Wan Q, Yi C, Xiao F, Liu Y, and Qi Y (2010). Nogo-B mediates HeLa cell adhesion and motility through binding of Fibulin-5. *Biochem Biophys Res Commun* **398**, 247–253.
- [34] Yang X, Liang L, Zhang XF, Jia HL, Qin Y, Zhu XC, Gao XM, Qiao P, Zheng Y, and Sheng YY (2013). MicroRNA-26a suppresses tumor growth and metastasis of human hepatocellular carcinoma by targeting interleukin-6-Stat3 pathway. *Hepatology* **58**, 158–170.
- [35] Rabinovich A, Medina L, Piura B, Segal S, and Huleihel M (2007). Regulation of ovarian carcinoma SKOV-3 cell proliferation and secretion of MMPs by autocrine IL-6. *Anticancer Res* **27**, 267–272.

- [36] Lou W, Ni Z, Dyer K, Tweardy DJ, and Gao AC (2000). Interleukin-6 induces prostate cancer cell growth accompanied by activation of Stat3 signaling pathway. *Prostate* **42**, 239–242.
- [37] Malinowska K, Neuwirt H, Cavarretta IT, Bektic J, Steiner H, Dietrich H, Moser PL, Fuchs D, Hobisch A, and Culig Z (2009). Interleukin-6 stimulation of growth of prostate cancer in vitro and in vivo through activation of the androgen receptor. *Endocr Relat Cancer* **16**, 155–169.
- [38] Santer FR, Malinowska K, Culig Z, and Cavarretta IT (2009). Interleukin-6 trans-signalling differentially regulates proliferation, migration, adhesion and maspin expression in human prostate cancer cells. *17*, 241–253.
- [39] Naugler WE, Sakurai T, Kim S, Maeda S, Kim KH, Elsharkawy AM, and Karin M (2007). Gender disparity in liver cancer due to sex differences in MyD88-dependent IL-6 production. *Science* **317**, 121.
- [40] Lee S, Lee M, Kim JB, Jo A, Cho EJ, Su JY, Lee JH, Yoon JH, and Kim YJ (2016). 17 β -estradiol exerts anticancer effects in anoikis-resistant hepatocellular carcinoma cell lines by targeting IL-6/STAT3 signaling. *Biochem Biophys Res Commun* **473**, 1247–1254.
- [41] Streeck KL, Tacke F, Leifeld L, Wüstefeld T, Graw A, Klein C, Kamino K, Spengler U, Kreipe H, and Kubicka S (2003). Interleukin 6/gp130-dependent pathways are protective during chronic liver diseases. *Hepatology* **38**, 218–229.
- [42] Cao F, Liu M, Zhang QZ, and Hao R (2016). PHACTR4 regulates proliferation, migration and invasion of human hepatocellular carcinoma by inhibiting IL-6/Stat3 pathway; 2016 .
- [43] He G and Karin M (2011). NF- κ B and STAT3—key players in liver inflammation and cancer. *Cell Res* **21**, 159–168.
- [44] Berasain C, Castillo J, Perugorria MJ, Latasa MU, Prieto J, and Avila MA (2009). Inflammation and liver cancer: new molecular links. *Ann NY Acad Sci* **1155**, 206.
- [45] Yu H, Pardoll D, and Jove R (2009). STATs in cancer inflammation and immunity: a leading role for STAT3. *Nat Rev Cancer* **9**, 798.
- [46] Yu H, Kortylewski M, and Pardoll D (2007). Crosstalk between cancer and immune cells: role of STAT3 in the tumour microenvironment. *Nat Rev Immunol* **7**, 41–51.
- [47] Xie TX, Wei D, Liu M, Gao AC, Ali-Osman F, Sawaya R, and Huang S (2004). Stat3 activation regulates the expression of matrix metalloproteinase-2 and tumor invasion and metastasis. *Oncogene* **23**, 3550–3560.
- [48] Xie TX, Huang FJ, Aldape KD, Kang SH, Liu M, Gershenwald JE, Xie K, Sawaya R, and Huang S (2006). Activation of stat3 in human melanoma promotes brain metastasis. *Cancer Res* **66**, 3188–3196.
- [49] Barré B, Vigneron A, Perkins N, Roninson IB, Gamelin E, and Coqueret O (2007). The STAT3 oncogene as a predictive marker of drug resistance. *Trends Mol Med* **13**, 4–11.
- [50] Kao JT, Feng CL, Yu CJ, Tsai SM, Hsu PN, Chen YL, and Wu YY (2015). IL-6, through p-STAT3 rather than p-STAT1, activates hepatocarcinogenesis and affects survival of hepatocellular carcinoma patients: a cohort study. *BMC Gastroenterol* **15**, 50.
- [51] Lu Z, Wang J, Zheng T, Liang Y, Yin D, Song R, Pei T, Pan S, Jiang H, and Liu L (2014). FTY720 inhibits proliferation and epithelial-mesenchymal transition in cholangiocarcinoma by inactivating STAT3 signaling. *BMC Cancer* **14**, 783–783.
- [52] Wang L and Yi TM (2009). IL-17 can promote tumor growth through an IL-6-Stat3 signaling pathway. *J Exp Med* **206**, 1457–1464.
- [53] Choudhari SR, Khan MA, Harris G, Picker D, Jacob GS, Block T, and Shailubhai K (2007). Deactivation of Akt and STAT3 signaling promotes apoptosis, inhibits proliferation, and enhances the sensitivity of hepatocellular carcinoma cells to an anticancer agent, Atiprimod. *Mol Cancer Ther* **6**, 2010–2011.
- [54] Fournier AE, GrandPre T, and Strittmatter SM (2001). Identification of a receptor mediating Nogo-66 inhibition of axonal regeneration. *Nature* **409**, 341–346.
- [55] Wang B, Xiao Z, Chen B, Han J, Gao Y, Zhang J, Zhao W, Wang X, and Dai Jianwu (2008). Nogo-66 promotes the differentiation of neural progenitors into astroglial lineage cells through mTOR-STAT3 pathway. *PLoS One* **3**, e1856.
- [56] Gao Y, Wang B, Xiao Z, Chen B, Han J, Wang X, Zhang J, Gao S, Zhao Y, and Dai J (2009). Nogo-66 regulates nanog expression through stat3 pathway in murine embryonic stem cells. *Stem Cells Dev* **19**, 53–60.
- [57] Fang Y, Yan J, Li C, Zhou X, Yao L, Pang T, Yan M, Zhang L, Mao L, and Liao H (2015). The Nogo/Nogo Receptor (NgR) signal is involved in neuroinflammation through the regulation of microglial inflammatory activation. *J Biol Chem* **290**, 28901.
- [58] In LS, Jieun Y, Ji-Young B, Yun-Ji J, Jin-Ah K, Jong Soon K, Hong PS, Kyum KS, and Song-Kyu P (2015). NgR1 expressed in P19 embryonal carcinoma cells differentiated by retinoic acid can activate STAT3. *Korean J Physiol Pharmacol* **19**, 105–109.
- [59] Fang Y, Yao L, Li C, Wang J, Wang J, Chen S, Zhou XF, and Liao H (2016). The blockage of the Nogo/NgR signal pathway in microglia alleviates the formation of A β plaques and tau phosphorylation in APP/PS1 transgenic mice. *J Neuroinflammation* **13**, 56.